Resolving spatial and energetic distributions of trap states in metal halide perovskite solar cells

March 30 2020, by Thamarasee Jeewandara

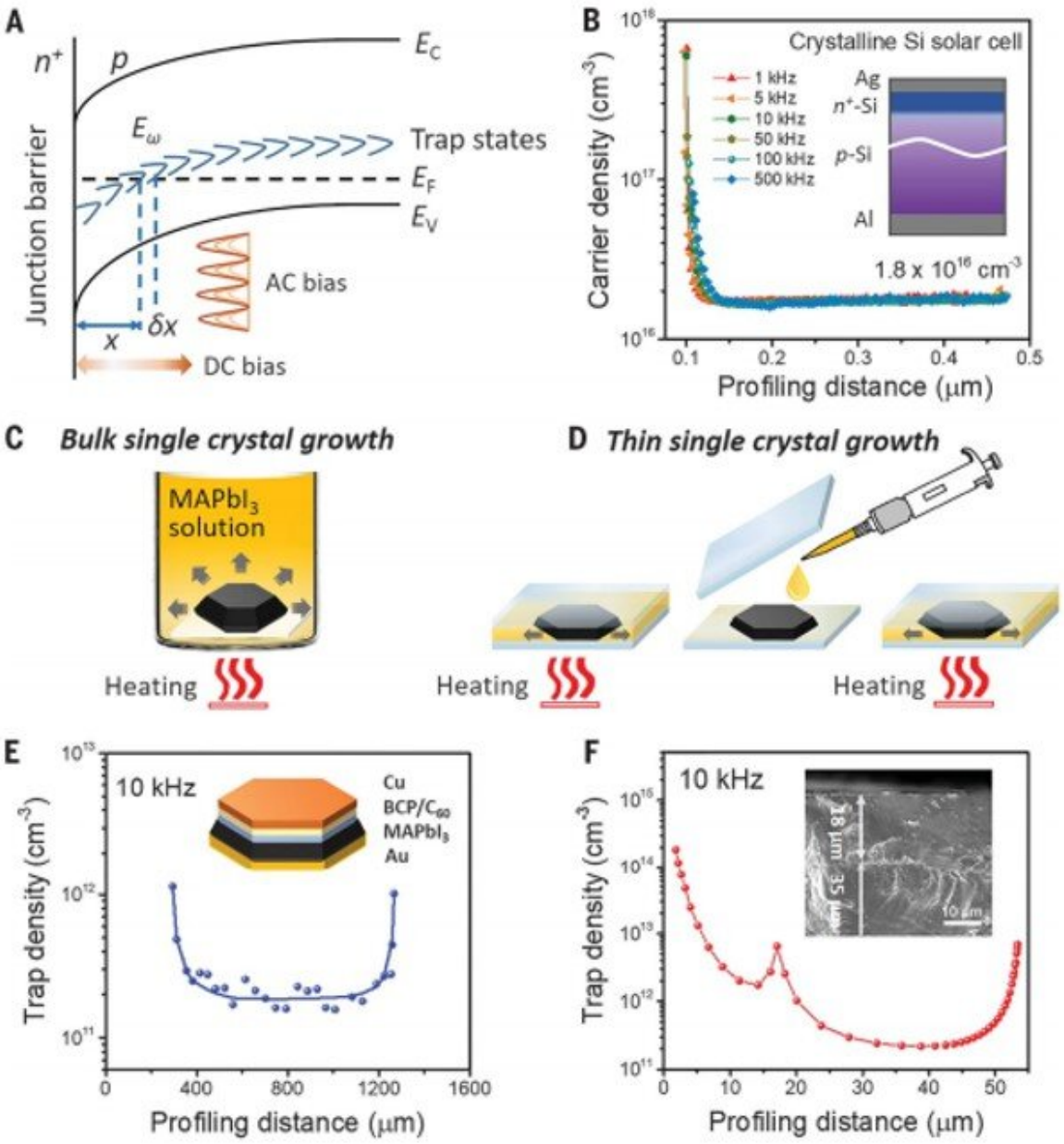

DLCP technique. (A) Schematic of band bending of a p-type semiconductor with deep trap states in an n+ -p junction. X denotes the distance from the junction barrier where the traps may be able to dynamically change their charge states with the ac bias dV. dX denotes the differential change of X with respect to dV. Ew is the demarcation energy determined by Ew = kTln(w0/w) (where k is the Boltzmann's constant). EC, EV, and EF indicate the conduction band edge, valence band edge, and Fermi level, respectively. (B) Dependence of the carrier

density on the profiling distance of a Si solar cell at different ac frequencies measured by DLCP. The inset shows the schematic of the device structure. (C) Schematic of the synthesis of a bulk MAPbI3 single crystal in an open-air solution. (D) Schematic of the synthesis of a double-layer MAPbI3 thin single crystal using the space-confined growth method. (E) Dependence of the trap density on the profiling distance of a MAPbI3 single crystal measured by DLCP. The inset shows the device structure. (F) Dependence of the trap density on the profiling distance of a double-layer MAPbI3 thin single crystal. The inset shows the cross-sectional SEM image of the double-layer MAPbI3 thin single crystal. The thicknesses of the top and bottom single crystals were 18 and 35 mm, respectively. Credit: Science, doi: 10.1126/science.aba0893

In a new report published on *Science*, Zhenyi Ni and a research team in applied physical sciences, mechanical and materials engineering and computer and energy engineering in the U.S. profiled spatial and energetic distributions of trap states or defects in metal halide perovskite single-crystalline polycrystalline solar cells. The researchers credited the photovoltaic performance of metal halide perovskites (MHPs) to their high optical absorption coefficient, carrier mobility, long charge-diffusion length and small Urbach energy (representing disorder in the system). Theoretical studies have demonstrated the possibility of forming deep charge traps at the material surface due to low formation energy, structural defects and grain boundaries of perovskites to guide the development of passivation techniques (loss of chemical reactivity) in perovskite solar cells. Charge trap states play an important role during the degradation of perovskite solar cells and other devices. Understanding the distribution of trap states in their space and energy can clarify the impact of charge traps (defects) on charge transport in perovskite materials and devices for their optimal performance.

Scientists have broadly used thermal admittance spectroscopy (TAS) and thermally stimulated current (TSC) methods to measure the energy-

dependent trap density of states (tDOS) within perovskite solar cells. The methods can generally reach a trap depth approximating 0.55 eV—deep enough to make efficient solar cells. To detect deeper trap states that exist within wide-band gap perovskites, researchers have used techniques such as surface photovoltage spectroscopy and sub-band gap photocurrent. However, most techniques cannot be applied to already completed solar devices to measure the spatial distribution of trap-states. In this work, Ni et al. demonstrated the drive-level capacitance profiling method (DLCP) – an alternate capacitance-based technique to provide well-characterized spatial distributions of carrier and trap-densities in perovskites. The scientists mapped the spatial and energetic distribution of trap-states within perovskite single crystals and polycrystalline thin films for straightforward comparison.

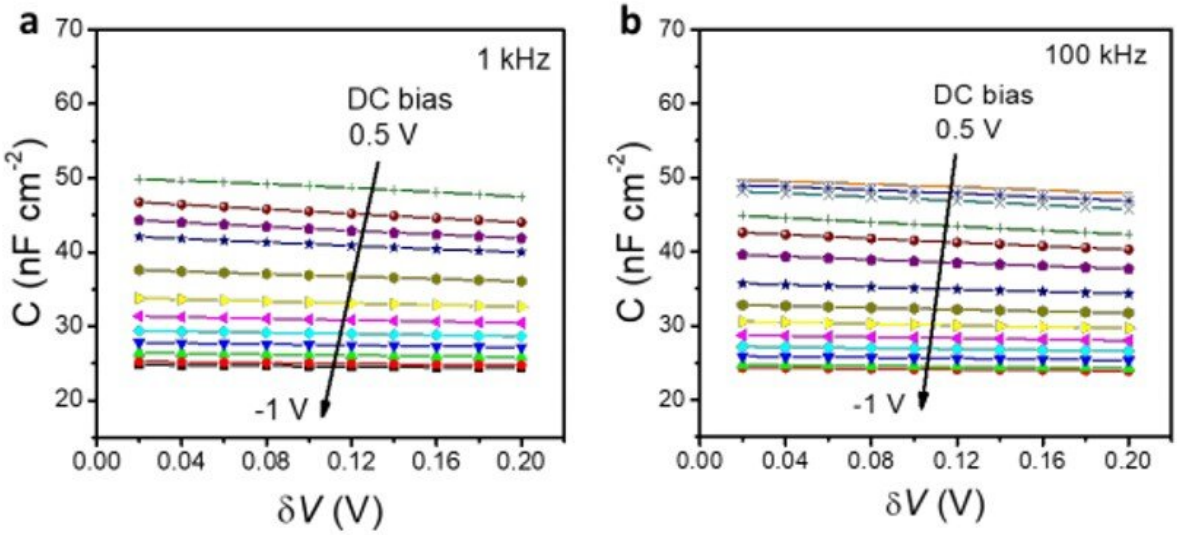

Variation of the junction capacitance with the amplitude of the AC biases for a Si solar cell. Variation of the junction capacitance (C) of a Si solar cell with respect to the amplitude of the AC biases (δV) under different DC biases measured at AC frequencies of (a) 1 kHz and (b) 100 kHz. Credit: Science, doi: 10.1126/science.aba0893

The team developed the DLCP (drive-level capacitance profiling) method to study the spatial distribution of defects in the band gap of amorphous and polycrystalline semiconductors such as amorphous silicon. The method could directly determine the carrier density to include both free carrier density and trap density within the band gap of semiconductors as well as their distribution in space and energy. They estimated the trap density by subtracting the estimated free carrier density measured at high alternating current (ac) frequencies from the total carrier density measured at low ac frequency. The technique allowed the team to derive the energetic distribution of trap states. To validate the accuracy of the carrier density measured using the DLCP method, the scientists performed DLCP measurements on a silicon solar cell fabricated on a p-type crystalline Si (p-Si) wafer with a n-type diffusion layer Si (n^+) on top. The measurement was consistent with the dopant concentration of the p-Si wafer obtained from the conductivity measurement to validate the accuracy of the carrier density measured using DLCP.

To profile the carrier and trap densities using DLCP, the researchers investigated across a device from one electrode to the counter-electrode to understand the location of junctions in planar-structured perovskite solar cells. The team conducted several experiments and observed that perovskite cells typically maintained a n^+-P junction between device constituents. In order to determine the profile depth corresponding to the physical material depth, Ni et al. constructed a device containing a double-layer of methyl ammonium lead iodide ($MAPbI_3$) thin crystals to locate the charge traps. When they profiled the trap density of the engineered device, they obtained a peak in the trap density at a profiling distance of 18 μm.

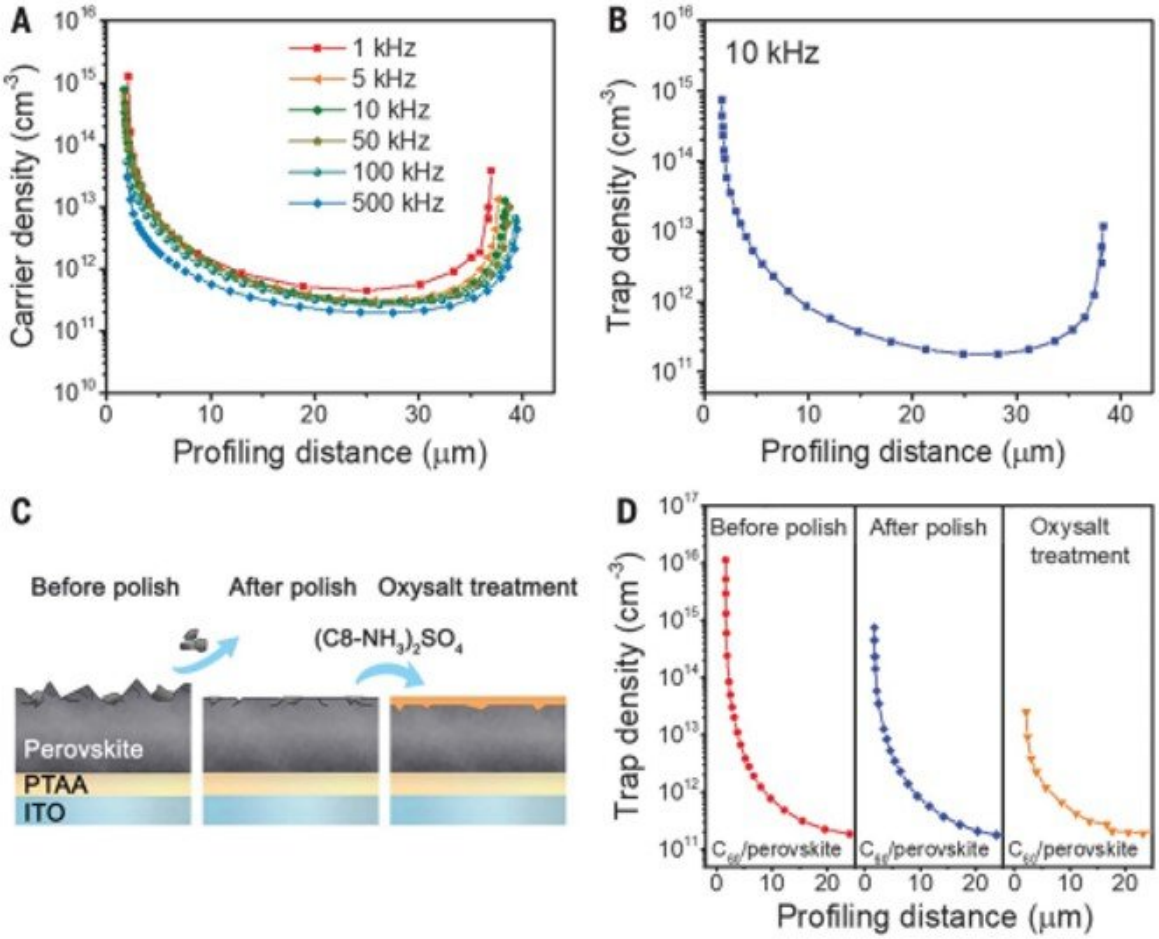

Spatial distributions of trap states in a MAPbI3 thin single crystal. (A) Dependence of the carrier density on the profiling distance of a 39-mm-thick MAPbI3 thin single crystal at different ac frequencies, as measured by DLCP. (B) Dependence of the trap density on the profiling distance of a MAPbI3 thin single crystal measured at an ac frequency of 10 kHz. The carrier density measured at 500 kHz is regarded as free carriers. (C) Schematics of a MAPbI3 thin single crystal on a PTAA/ITO substrate before mechanical polish, after mechanical polish, and after oxysalt [(C8–NH3)2SO4] treatment. (D) Trap density near the junction barrier of a MAPbI3 thin single crystal before mechanical polish, after mechanical polish, and after oxysalt treatment. Credit: Science, doi: 10.1126/science.aba0893

The team then studied the trap distribution in perovskite single-crystal solar cells and observed the highest power conversion efficiency (PCE) of the first reported $MAPbI_3$ single-crystal solar cell to be only 17.9 percent; far lower than that of polycrystalline solar cells. They were unaware of the underlying mechanism that limited carrier diffusion in thin crystals and conducted DLCP measurements to investigate the relationship of trap density and trap distributions using synthetic-crystal methods. The team observed the spatial distribution of carrier densities throughout a typical $MAPbI_3$ thin single crystal, which they synthesized using a space-confined growth method at different frequencies, and noted increasing carrier density with decreasing ac frequency, indicating the existence of charge traps in the $MAPbI_3$ thin single crystal.

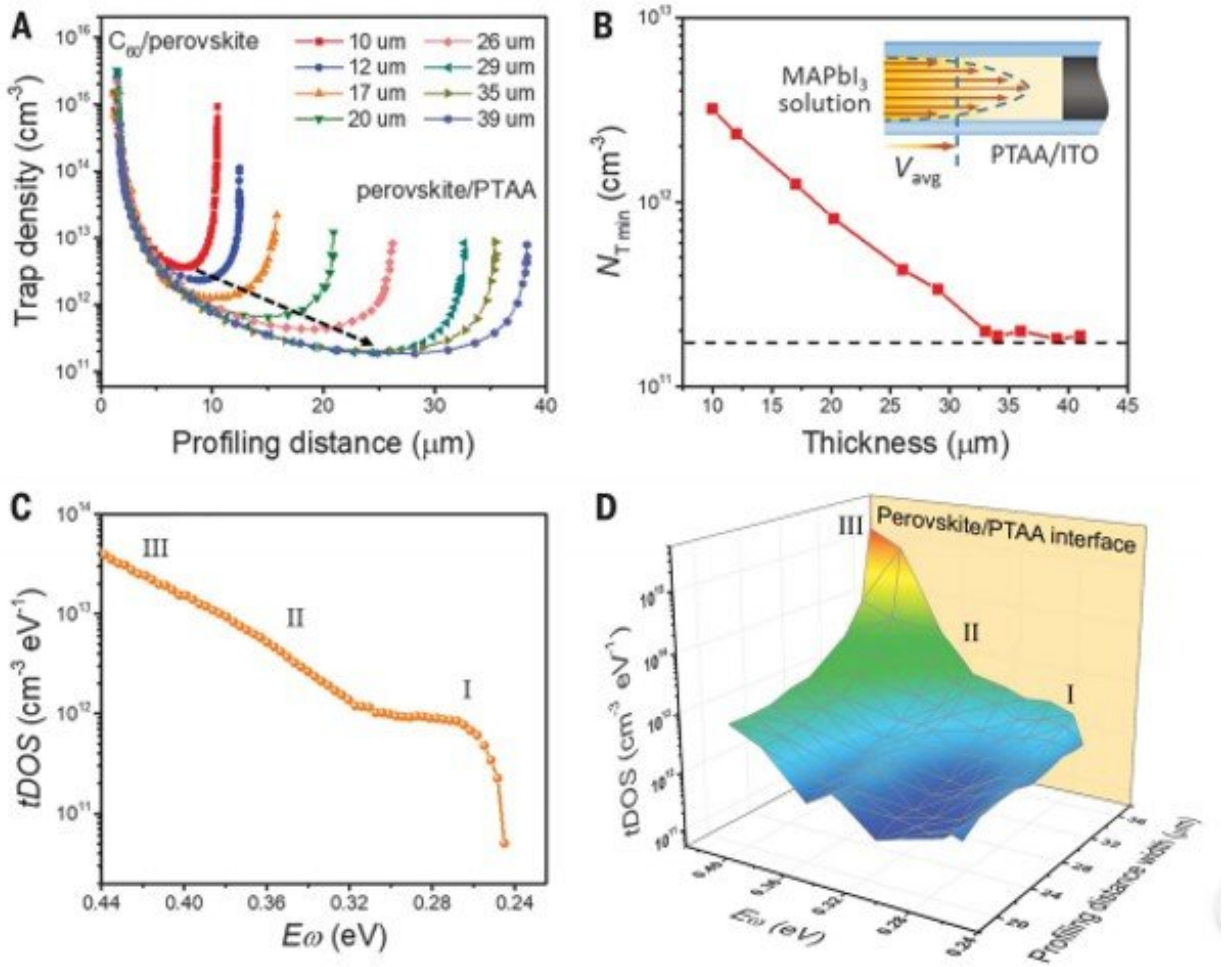

Thickness-dependent trap density distributions in MAPbI3 thin single crystals. (A) Dependence of the trap densities on the profiling distances of MAPbI3 thin single crystals with different crystal thicknesses measured at an ac frequency of 10 kHz. The location of the MAPbI3/C60 interface for each crystal is aligned for comparison. The black dashed arrow indicates the trend of the change of minimal trap density NT min in MAPbI3 single crystals with different thicknesses. (B) Dependence of the NT min in the MAPbI3 thin single crystal on the crystal thickness. The horizontal dashed line indicates the NT min value in a bulk MAPbI3 single crystal. The inset shows a schematic of the laminar flow of the precursor solution between two PTAA/ITO glasses during the growth of the crystal. The arrows denote the direction of the laminar flow of the precursor solution, and the length of the arrow denotes the laminar flow velocity. (C) tDOS of a MAPbI3 thin single crystal, as measured by the TAS method. The thickness

of the MAPbI3 thin single crystal was 39 mm. (D) Spatial and energy mapping of the densities of trap states in the MAPbI3 thin single crystal, as measured by DLCP. Credit: Science, doi: 10.1126/science.aba0893

To understand the origin of deep trap density at the perovskite interface, the team used high-resolution transmission electron microscopy and examined perovskite samples of different compositions. They compared trap density distributions between perovskite single crystals and polycrystalline thin films with varying compositions. The trap density distributions for thin single crystals were several orders of magnitude lower than that in polycrystalline thin films. The results showed the importance of adequate surface modification processes to reduce trap densities in perovskite single crystals at the interface of polycrystalline thin films to enhance device performance. The results point toward an important direction to boost the performance of perovskite solar cells and other electronic devices by reducing the trap density at the interface.

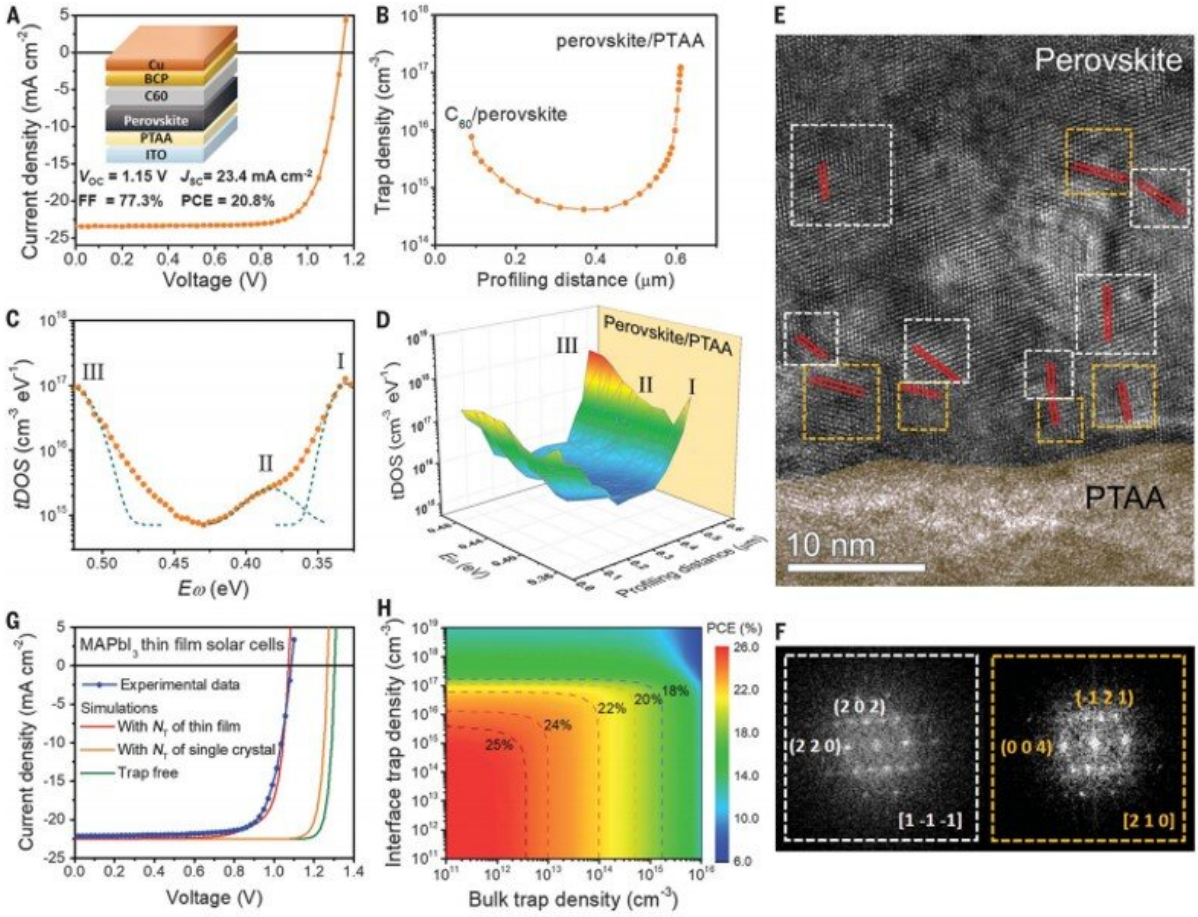

Spatial and energetic distributions of trap states in perovskite thin films. (A) J-V curve of the Cs0.05FA0.70MA0.25PbI3 thin-film solar cells. The inset shows the device structure. (B) Dependence of the trap density on the profiling distance for the perovskite thin film in the solar cell measured at an ac frequency of 10 kHz. (C) tDOS of the perovskite thin-film solar cell, as measured by the TAS method. (D) Spatial and energy mapping of the densities of trap states of the perovskite thin film in the solar cell, as measured by DLCP. (E) Cross-sectional HR-TEM image of the stack of perovskite and PTAA. The dashed squares mark the areas where the fast Fourier transforms of the lattices were performed, with white and yellow indicating zone axes of [1 −1 −1] and [2 1 0], respectively. The red lines denote the orientation of the facets. (F) Fast Fourier transforms of the areas indicated in (E). (G) Measured and simulated J-V curves of planar-structured solar cells based on MAPbI3 polycrystalline thin films. The thin-film (single crystal) bulk and interface trap densities were adopted for the simulations. (H) Dependence of the PCE of the MAPbI3 thin-film solar cell on

the bulk and interface trap densities. The dashed lines denote the contour lines of certain PCE values, which are noted. Credit: Science, doi: 10.1126/science.aba0893

In this way, Zhenyi Ni and colleagues used the solar cell capacitance simulator to simulate the thin-film and single-crystal perovskite solar cells with varying trap densities. The range of traps measured with DLCP measurements were deep enough to predict the behavior of solar cells and reduce the bulk trap density of materials and increase the power conversion efficiency (PCE) up to 20 percent. By decreasing the interface trap density, they increased the PCE values closer to the PCE observed for a trap-free thin film solar cell. The data simulated for single-crystal solar cells agreed well with experiments, showing that the PCE of the single-crystal solar cell could be further improved at the device interface to harvest more sunlight.

More information: Zhenyi Ni et al. Resolving spatial and energetic distributions of trap states in metal halide perovskite solar cells, *Science* (2020). DOI: 10.1126/science.aba0893

James M. Ball et al. Defects in perovskite-halides and their effects in solar cells, *Nature Energy* (2016). DOI: 10.1038/nenergy.2016.149

Qi Jiang et al. Surface passivation of perovskite film for efficient solar cells, *Nature Photonics* (2019). DOI: 10.1038/s41566-019-0398-2

energetic-states-metal-halide.html